LBL-12469
SAC-33
UC-70

LBL--12469

DE83 014919

NUMERICAL MODELING TO ASSESS POSSIBLE INFLUENCE OF THE MINE OPENINGS ON FAR-FIELD IN-SITU STRESS MEASUREMENTS AT STRIPA

T. Chan, V. Guvanasen, and N. Littlestone

Earth Sciences Division
Lawrence Berkeley Laboratory
University of California
Berkeley, California 94720

March 1981

This work was supported by the Assistant Secretary for Nuclear Energy, Office of Waste Isolation of the U.S. Department of Energy under contract DE-AC03-76SF00098. Funding for this project is administered by the Office of Nuclear Waste Isolation at Battelle Memorial Institute.

PREFACE

This report is one of a series documenting the results of the Swedish-American cooperative research program in which the cooperating scientists explore the geological, geophysical, hydrological, geochemical, and structural effects anticipated from the use of a large crystalline rock mass as a geologic repository for nuclear waste. This program has been sponsored by the Swedish Nuclear Power Utilities through the Swedish Nuclear Fuel Supply Company (SKBF), and the U.S. Department of Energy (DOE) through the Lawrence Berkeley Laboratory.

The principal investigators are L.B. Nilsson and O. Degerman for SKBF, and N.G.W. Cook, P.A. Witherspoon, and J.E. Gale for LBL. Other participants will appear as authors of the individual reports.

Previous technical reports in this series are listed below.

1. Swedish-American Cooperative Program on Radioactive Waste Storage in Mined Caverns by P.A. Witherspoon and O. Degerman. (LBL-7049, SAC-01).

2. Large Scale Permeability Test of the Granite in the Stripa Mine and Thermal Conductivity Test by Lars Lundstrom and Haken Stille. (LBL-7052, SAC-02).

3. The Mechanical Properties of the Stripa Granite by Graham Swan. (LBL-7074, SAC-03).

4. Stress Measurements in the Stripa Granite by Hans Carlsson. (LBL-7078, SAC-04).

5. Borehole Drilling and Related Activities at the Stripa Mine by P.J. Kurfurst, T. Hugo-Persson, and G. Rudolph. (LBL-7080, SAC-05).

6. A Pilot Heater Test in the Stripa Granite by Hans Carlsson. (LBL-7086, SAC-06).

7. An Analysis of Measured Values for the State of Stress in the Earth's Crust by Dennis B. Jamison and Neville G.W. Cook. (LBL-7071, SAC-07).

8. Mining Methods Used in the Underground Tunnels and Test Rooms at Stripa by B. Andersson and P.A. Halen. (LBL-7081, SAC-08).

9. Theoretical Temperature Fields for the Stripa Heater Project by T. Chan, Neville G.W. Cook, and C.F. Tsang. (LBL-7082, SAC-09).

10. Mechanical and Thermal Design Considerations for Radioactive Waste Repositories in Hard Rock. Part I: An Appraisal of Hard Rock for Potential Underground Repositories of Radioactive Waste by N.G.W. Cook; Part II: In Situ Heating Experiments in Hard Rock: Their Objectives and Design by N.G.W. Cook and P.A. Witherspoon. (LBL-7073, SAC-10).

11. Full-Scale and Time-Scale Heating Experiments at Stripa: Preliminary Results by N.G.W. Cook and M. Hood. (LBL-7072, SAC-11).

12. Geochemistry and Isotope Hydrology of Groundwaters in the Stripa Granite: Results and Preliminary Interpretation by P. Fritz, J.F. Barker, and J.E. Gale. (LBL-8285, SAC-12).

13. Electrical Heaters for Thermo-Mechanical Tests at the Stripa Mine by R.H. Burleigh, E.P. Binnall, A.O. DuBois, O.O. Norgren, and A.R. Ortiz. (LBL-7063, SAC-13).

14. Data Acquisition, Handling, and Display for the Heater Experiments at Stripa by Maurice B. McEvoy. (LBL-7063, SAC-14).

15. An Approach to the Fracture Hydrology at Stripa: Preliminary Results by J.E. Gale and P.A. Witherspoon. (LBL-7079, SAC-15).

16. Preliminary Report on Geophysical and Mechanical Borehole Measurements at Stripa by P. Nelson, B. Paulsson, R. Rachiele, L. Andersson, T. Schrauf, W. Hustrulid, O. Duran, and K.A. Magnussen. (LBL-8280, SAC-16).

17. Observations of a Potential Size-Effect in Experimental Determination of the Hydraulic Properties of Fractures by P.A. Witherspoon, C.H. Amick, J.E. Gale, and K. Iwai. (LBL-8571, SAC-17).

18. Rock Mass Characterization for Storage in Nucler Waste in Granite by P.A. Witherspoon, P. Nelson, T. Doe, R. Thorpe, B. Paulsson, J.E. Gale, and C. Forster. (LBL-8570, SAC-18).

19. Fracture Detection in Crystalline Rock Using Ultrasonic Shear Waves by K.H. Waters, S.P. Palmer, and W.F. Farrell. (LBL-7051, SAC-19).

20. Characterization of Discontinuities in the Stripa Granite--Time Scale Heater Experiment by R. Thorpe. (LBL-7083, SAC-20).

21. Geology and Fracture System at Stripa by A. Okliewicz, J.E. Gale, R. Thorpe, and B. Paulsson. (LBL-8907, SAC-21).

22. Calculated Thermally Induced Displacements and Stresses for Heater Experiements at Stripa by T. Chan and N.G.W. Cook. (LBL-7061, SAC-22).

23. Validity of Cubic Law for Fluid Flow in a Deformable Rock Fracture by P.A. Witherspoon, J. Wang, K. Iwai, and J.E. Gale. (LBL-9557, SAC-23).

24. Determination of In-Situ Thermal Properties of Stripa Granite from Temperature Measurements in the Full-Scale Heater Experiments: Methods and Primary Results by J. Jeffry, T. Chan, N.G.W. Cook and P.A. Witherspoon. (LBL-8424, SAC-24).

25. Instrumentation Evaluation, Calibration, and Installation for Heater Tests Simulating Nuclear Waste in Crystalline Rock, Sweden by T. Schrauf, H. Pratt, E. Simonson, W. Hustrulid, P. Nelson, A. DuBois, E. Binnall, and R. Haught. (LBL-8313, SAC-25)

26. Part I: Some Results From a Field Investigation of Thermo-Mechanical Loading of a Rock Mass When Heater Canisters are Emplaced in the Rock by M. Hood. Part II: The Application of Field Data from Heater Experiments Conducted at Stripa, Sweden for Repository Design by M. Hood, H. Carlsson, and P.H. Nelson. (LBL-9392, SAC-26).

27. Progress with Field Investigations at Stripa by P.A. Witherspoon, N.G.W. Cook, and J.E. Gale (LBL-10559, SAC-27).

28. A Laboratory Assessment of the Use of Borehole Pressure Transients to Measure the Permeability of Fractured Rock Masses by C.B. Forster and J.E. Gale. (LBL-8674, SAC-28).

29. Thermal and Thermomechanical Data for In Situ Heater Experiments at Stripa, Sweden by T. Chan, E. Binnall, P. Nelson, O. Wan, C. Weaver, K. Ang, J. Braley, and M. McEvoy. (LBL-11477, SAC-29).

30. The Effect of Radon Transport in Groundwater Upon Gamma Ray Borehole Logs by P.H. Nelson, R. Rachiele, and A. Smith. (LBL-11180, SAC-30).

31. Strength and Permeability Tests on Ultra-Large Stripa Granite Core by R. Thorpe, D.J. Watkins, W.E. Ralph, R. Hsu, and S. Flexser. (LBL-11203, SAC-31).

32. Ultrasonic and Acoustic Emission Results from the Stripa Heater Experiments. Part I: A Cross-Hole Investigation of a Rock Mass Subjected to Heating by B.N.P. Paulsson and M.S. King. Part II: Acoustic Emission Monitoring During Cool-Down of the Stripa Heater Experiment by R. Rachiele. (LBL-10975, SAC-32).

TABLE OF CONTENTS

LIST OF FIGURES

LIST OF TABLES

ABSTRACT

Finite element analyses were carried out to assess the possible effects of the Stripa mine openings on the in situ stress measured in a 400-m-deep borehole drilled from the surface. For this assessment, four 2-dimensional cases were modeled. These cases variously included two horizontal sections, and two separate, idealized vertical sections. An iron ore body in the mine was assumed to be completely extracted, thereby providing conservative estimates of stress concentration effects.

Since no in situ stress measurements were made before mining, overburden weight and horizontal stresses measured by hydrofracturing were assumed to be the pre-mining state of stress. The stress state resulting from excavation of the mine was calculated by the finite element model. In the cases using horizontal sections, the model predicted a stress concentration factor at the borehole of approximately 1.15, which is negligible considering the difficulty of obtaining accurate stress measurements. For the vertical sections the model predicted higher stress concentration factors at depths less than 200 m. This was expected because the vertical sections chosen brought the borehole unrealistically close to the mine openings, thereby leading to overly conservative estimates.

In general, deviations in the magnitudes and orientations of the calculated redistributed principal stresses from the assumed pre-mining state of stress were found to be comparable to the scatter of overcoring data. It is, therefore, recommended that, for near-field stress calculations, the vertical stress due to overburden weight and the horizontal stresses measured by

hydrofracturing at the borehole be considered the unperturbed far-field in situ state of stress.

1.0 INTRODUCTION

1.1 Background and Objective

Over the past three years, thermomechanical, hydrological, and other investigations have been conducted at a depth of approximately 340 m in a granite* body adjacent to a depleted iron ore mine at Stripa, Sweden (Witherspoon et al., 1981), to see if such bodies can be used as nuclear waste repositories. The present work is the first part of a project to exhaustively analyze the thermomechanical data obtained from the in situ heater test.

In the heater tests, electrical heaters were placed in drill-holes in the floor of specially excavated experimental drifts (tunnels) to simulate the thermal energy resulting from the decay of radioactive wastes. Temperatures, displacements, and stresses were measured in the rock. This report focuses on stresses. Since the thermomechanical loading was applied after the rock had been perturbed by removal of a large portion of the ore body, by the excavation of the experimental drifts, and by the drilling of boreholes, the instantaneous state of stress at a point in the rock during the heater tests was a result of the following (chronologically ordered) components: (i) the pre-mining, pre-excavation stress, (ii) the mining-induced stress, (iii) the stresses induced by drift excavation and borehole drilling, and (iv) the thermally induced stress. Of these, the first three components were present before heating, and only stress changes, i.e., component (iv) above, were measured during the experiments (see Schrauf et al., 1979, for details of instrumentation).

---

*The term "granite" is used loosely here. The rock type is a "quartz monzonite" or "monzogranite." See Olkiewicz et al. (1979) for mineral composition.

If the rock is linear elastic, i.e., its properties are independent of stress, then the thermally induced stresses can be calculated from the known system geometry, from the thermal field obtained in a separate calculation, and from the rock properties measured under room conditions. That was, indeed, the approach taken in the preliminary calculations (Chan and Cook, 1979). Comparison with field data showed that there were significant discrepancies. Subsequently, limited laboratory data became available on the temperature and stress dependence of the mechanical and thermomechanical properties of Stripa granite, and finite element analyses were carried out incorporating temperature-dependent properties (Chan, Hood and Board, 1980; Chan, Littlestone and Wan, 1980). The results were encouraging.

To incorporate stress-dependent properties into a numerical model correctly, it is necessary to know the spatial distribution of the absolute stress. Since stress measurements are invasive, it is clearly impossible to measure the absolute stress at every point. A reasonable approach is to measure the pre-mining, pre-excavation state of stress at a number of points and obtain the spatial distribution of the mining and excavation induced stress changes by numerical modeling. Since the experimental site was near an existing mine, the in situ stress measurements should be made as far away from the underground openings as possible. Other considerations (to be discussed in the next subsection), however, have made it necessary to measure the in situ stress in a borehole drilled from the surface at a distance which may not be completely outside the zone of influence of the mining-induced stress concentration. The purpose of this work was to determine, by numerical modeling, whether the measured in situ stress, which is actually a combination of components (i), (ii), and (iii) above, differs significantly from the

pre-mining, pre-excavation stress. If the differences are large, further work would have to be done to estimate the true pre-mining, pre-excavation stress.

1.2 Location, Geometry and Geologic Structure

In situ stress measurements were made (Doe et al., 1981) in a vertical hole labeled SBH-4, about 300 m north of the underground test site, as illustrated in the sub-till surface map (Fig. 1). There are three major types of rock, namely, leptite (a Precambrian metavolcanic sediment), the iron ore, and granite. The iron ore, which has largely been removed, lies in the leptite formation. The underground test site, where thermomechanical and hydrological tests were conducted, lies entirely in granite at the test level (about 340 m depth) although the surface projection of the test site falls outside of the outcrop of the granitic pluton. The location for the stress measurement borehole was a compromise between two conflicting criteria: (i) the borehole should be as far away as possible from the mine openings, and (ii) it should lie in the same granitic pluton as the underground test site.

The almost entirely mined-out iron ore deposits, indicated by the dark areas in Fig. 1, strike approximately northeast. The surface outcrop of this ore body is about 700 m from SBH-4, at its nearest point. However, as shown in the 3-D drawing of Fig. 2(a), the envelope of the mine workings slopes and spreads out in such a way that, at its closes point -- the 360 m level -- it is less than 400 m from SBH-4.

1.3 Scope of Present Study

Two methods were used to measure in situ stress in SBH-4, hydrofracturing and overcoring (Doe et al., 1981). Hydrofracturing gives the secondary

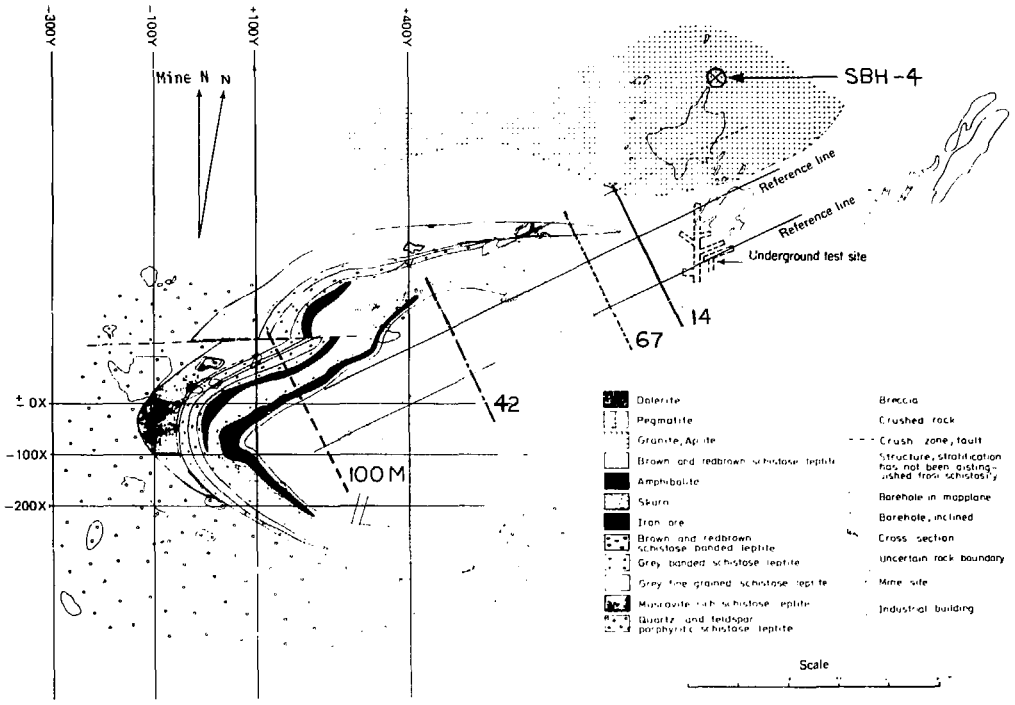

Fig. 1. Surface map of the Stripa mine showing the location of the underground test site, the SBH-4 hole, and mine coordinates.

XBL 816-3228

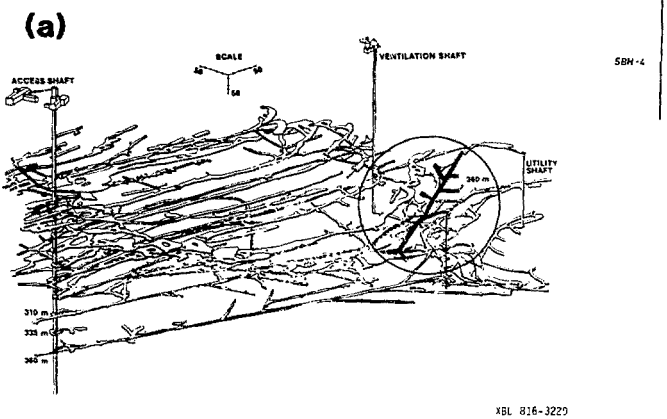

Fig. 2(a). Three-dimensional diagram showing excavated regions, the underground test site, and SBH-4 location.

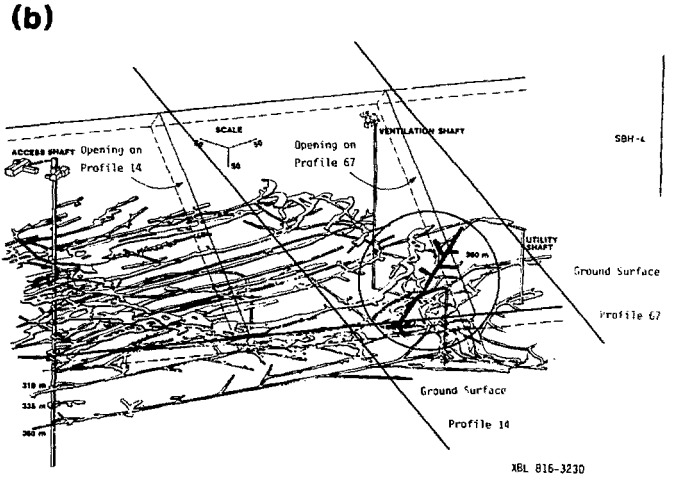

Fig. 2(b). Projection of the rectangular-slab idealization of the mine excavation, superimposed on Fig. 2(a). See also Fig. 6(a).

principal stresses in the horizontal plane. Overcoring measures the full three-dimensional stress tensor. Measurements were made with each method at a variety of depths down to about 400 m. There was considerable scatter, particularly in the overcoring measurements.

Because the overcoring measurements are basically point measurements, whereas hydrofracturing gives the mean stress over the area of the fracture, the hydrofracturing measurements were primarily used in this study. Only the overcoring measurements, however, can indicate if the mining excavation affected the orientation of the principal stresses in 3-D space.

The present study focuses on the far-field state of stress. This allowed us to simplify calculations by ignoring the effect of the drifts excavated for the underground experiments, especially since these drifts are much smaller than the old mine openings. Hereafter, therefore, the term "excavation" will refer exclusively to mining excavations.

In view of the extremely complicated geometry of the mine openings and the uncertainties in rock mass properties, it was impractical to model the 3-D configuration at this stage. Therefore, as a first step, approximate 2-D finite element models of horizontal and vertical sections were used. In these models the ore body was assumed to be completely extracted, providing upper-bound estimates of any stress concentration that might have affected the in situ stress measurements. The results of 2-D analyses should indicate whether 3-D modeling would be necessary. Figure 2(b) illustrates one idealization of the mine openings superimposed upon a 3-D drawing of the actual openings.

It should be emphasized that ab initio calculation of in situ stress is impossible. The stress concentration factor (SCF) is used to quantify the effect of the excavation on the in situ stress. This factor is the ratio of the stress at any point after an excavation to the stress before excavation at the same point. With the linear rock properties assumed in these models, the SCF is affected by the relative, but not the absolute, magnitudes of the pre-excavation stress components.

The effect of mining was studied by assuming that the pre-mining vertical stress was determined by the weight of the overburden, a reasonable assumption. A linear fit from the hydrofracture data was used for the assumed horizontal stress. The effect of the mining excavations was then modeled. A calculated SCF close to 1.0 would suggest that these assumptions are reasonable; a value much different from 1.0 would suggest a need to modify them.

2.0 NUMERICAL MODELING

In calculating the in situ state of stress in an elastic rock medium with a mine opening, one can either (i) include the initial (pre-mining stress directly in the finite element formulation and then create the opening, or (ii) apply equivalent boundary loads to the medium in which the opening already exists. The finite element implementation of these two options is briefly reviewed in Section 2.1. Both methods were used in the present study. The general assumptions, geometric idealization, loading and boundary conditions, and material properties employed in the analysis of the Stripa stituation are presented in Section 2.2

2.1 Methods for Including Initial Stress in Finite Element Analysis

The instantaneous stress in an elastic body can be expressed as:

$$\underline{\sigma} = \underline{\underline{D}} \, (\underline{\varepsilon} - \underline{\varepsilon}_0) + \underline{\sigma}_0 \quad , \tag{1}*$$

where

$\underline{\sigma}$ = instantaneous stress (vector),

$\underline{\underline{D}}$ = elasticity matrtix,

$\underline{\varepsilon}$ = instantaneous strain (vector),

$\underline{\varepsilon}_0$ = initial strain (vector),

$\underline{\sigma}_0$ = initial stress (vector).

The finite element formulation of the problem of equilibrium (Zienkiewicz, 1977) leads to the equation:

$$\underline{\underline{K}} \, \underline{a} + \underline{f} = \underline{r} \, , \tag{2}$$

---

*Although stress is a tensor quantity, it is expedient to arrange the stress components in the form of a column vector.

where $\underline{\underline{K}}$ = system stiffness matrix,

$\underline{a}$ = nodal displacement vector,

$\underline{f}$ = distributed (body or surface) force vector,

$\underline{r}$ = external concentrated nodal force vector.

The force vector, $\underline{f}$, is given by

$$\underline{f} = -\int_V \underline{\underline{N}}^T \underline{b}\, dV - \int_A \underline{\underline{N}}^T \underline{t}\, dA - \int_V \underline{\underline{B}}^T \underline{\underline{D}}\, \underline{\varepsilon}_o\, dV + \int_V \underline{\underline{B}}^T \underline{\sigma}_o\, dV , \qquad (3)$$

where

$\underline{\underline{N}}^T$ = transpose of shape function matrix,

$\underline{b}$ = body force vector,

$\underline{t}$ = boundary traction,

$\underline{\underline{B}}^T$ = transpose of strain-displacement matrix (see below),

V = system volume,

A = surface enclosing V,

The matrix B relates the finite element approximation of the strain, ε, to the nodal displacements; thus:

$$\underline{\varepsilon} \approx \underline{\hat{\varepsilon}} = \underline{\underline{B}}\, \underline{a} . \qquad (4)$$

Solution of Eq. (2) yields the nodal displacements from which stress can be calculated using Eqs. (4) and (1).

2.1.1 Direct Inclusion of Initial Stress

The general method for including initial stress in finite element analysis is by implementing the full sets of Eqs. (1) - (4) above. This

formulation is valid for both linear and nonlinear elasticity, provided that, in the latter case, the various quantities in the equations are interpreted as incremental quantities or, alternatively, an iterative procedure is used. For a highly nonlinear rock, the excavation sequence can be simulated by sequential removal of the elements representing the excavation. This procedure is now considered standard. The interested reader should consult Zienkiewicz (1977) for details.

2.1.2 Boundary Loading

For linear elasticity, in the absence of other causes of initial strain, one has the initial condition

$$\underline{\sigma}_0 = \underline{\underline{D}}\,\underline{\varepsilon}_0 \quad . \tag{5}$$

Equation (1) then reduces to:

$$\underline{\sigma} = \underline{\underline{D}}\,\underline{\varepsilon} \quad , \tag{1'}$$

while Eq. (3) reduces to:

$$\underline{f} = -\int_V \underline{\underline{N}}^T \underline{b}\, dV - \int_A \underline{\underline{N}}^T \underline{t}\, dA \quad . \tag{3'}$$

The combined initial and excavation-induced stresses can be obtained by solving Eq. (2) in conjunction with Eqs. (1') and (3') with an appropriate boundary condition to simulate the initial (pre-mining) stress, $\underline{\sigma}_0$.
In practice, this can be effected by either (i) applying negative traction to the excavation boundary (Chan, 1979) or (ii) assuming the excavation boundary to be stress free and applying boundary loads to the external boundary of the system (see Section 2.2.2).

Simulation of initial stress by boundary loading is not quite correct since this would deform the rock even in the absence of any opening. If the point of interest is sufficiently far away from the boundary, however, the error introduced would be small by virture of St. Venant's principle.

2.2. Calculations

Calculations were undertaken for the horizontal and vertical sections shown in Figs. 3 and 4, respectively. In the analysis of the horizontal sections, the 176 m and 360 m levels were selected because the mined-out area is largest at the former level and nearest to the SBH-4 borehole at the latter. In situ stresses measured at SBH-4 were expected to deviate from the pre-mining state by the greatest amount at either of these two levels.

Vertical sections of mine openings shown in Fig. 4 are those intersected by profiles 14, 67, 42, and 100M (Fig. 2), which are normal to the strike of the ore body. This orientation was chosen because theoretical solutions for stress distribution about ellipsoidal cavities (Sadowsky and Sternberg, 1949) had demonstrated that the zone of influence about 3-D openings is more nearly proportional to the radius of the shortest dimension of the opening than to the longest. The chosen orientation allows the shortest possible opening dimension so that the size of the zone of influence as well as the magnitude of stress redistributed by the mine opening will not be unrealistically overestimated.

General assumptions made in the analyses were that (i) the entire ore body had been removed and (ii) all openings were infinitely long. The second assumption permitted the problems to be reduced to two dimensions.

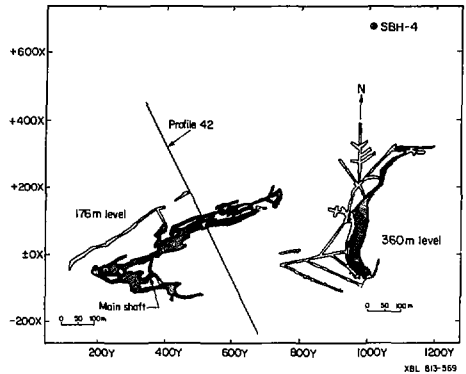

Fig. 3. Horizontal sections showing excavated regions (shaded) at 176 and 360 m levels.

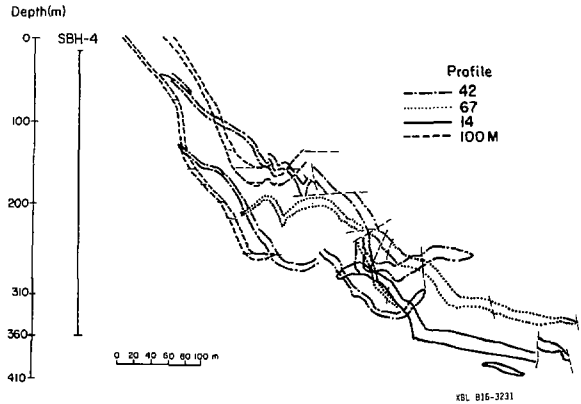

Fig. 4. Vertical section approximately normal to strike of ore body showing superposed excavated regions on profiles 42, 67, 14 and 100M, indicated by different types of lines corresponding to those in Fig. 1. Viewing direction = SW to NE.

This approach is conservative and should yield results indicating the maximum possible alterations of initial stresses due to mining.

2.2.1 Geometrical Idealizations

Geometrical idealizations of the mined-out areas in Figs. 3 and 4 are shown in Figs. 5 and 6, respectively.

In the analysis of the vertical sections, two different geometrical approximations were adopted: a single rectangle and two parallel rectangles as shown in Fig. 6. The single rectangle circumscribes profiles of all the mine openings while the double rectangles more accurately represent the geometrical characteristics of the profiles of the mined-out ore body.

2.2.2 Loading and Boundary Conditions

Loading conditions for all cases in this report were based on results from hydraulic fracturing experiments in SBH-4 (Doe et al., 1981). The mean orientation of the maximum horizontal stress is indicated by the experimental results to be N 65° W (Fig. 7).

The vertical stress component was assumed to be due totally to lithostatic stress. On the basis of the value of Stripa granite density given by Swan (1978) (density = 2622 kg/m^3), the distribution of vertical stress as a function of depth z (positive downwards) was found to be:

$$\sigma_v = 25721\ z \quad \text{(Pa)} \quad . \qquad (6)^*$$

*The large numbers of digits in Eqs. (6) and (7) are given to facilitate numerical evaluation and should not be taken as an indication of the accuracy of the data.

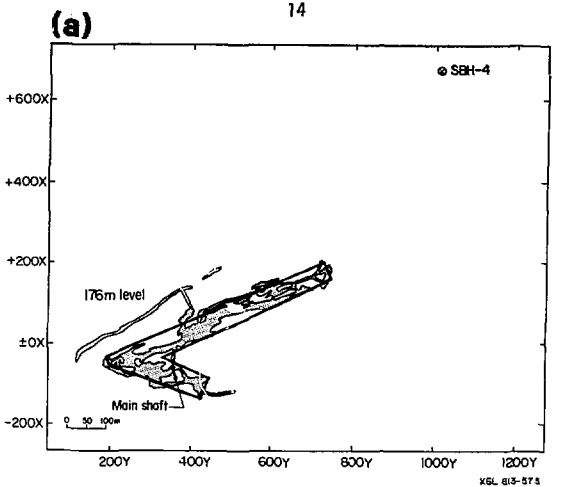

Fig. 5(a). Idealized geometry (bold line) of the horizontal section at the 176 m level. Direction of the X-axis corresponds to mine North.

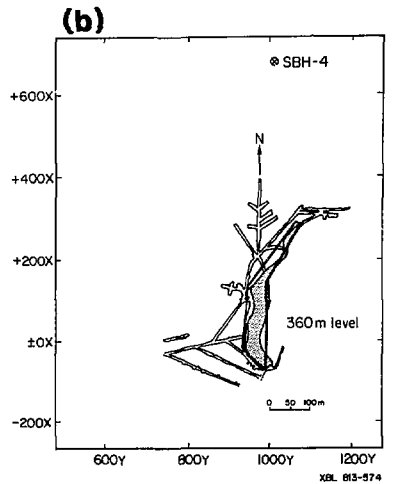

Fig. 5(b). Idealized geometry (bold line) of the horizontal section at the 360 m level. Direction of X-axis corresponds to mine North.

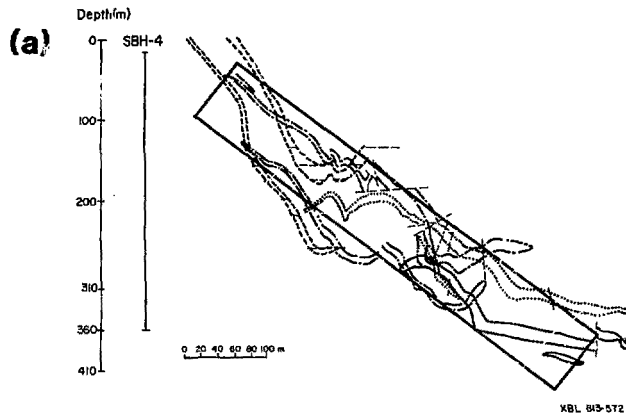

Fig. 6(a). Idealized geometry (bold line) of the superposed vertical sections in Fig. 4 -- single rectangle. See also Fig. 2(b) for 3D projection.

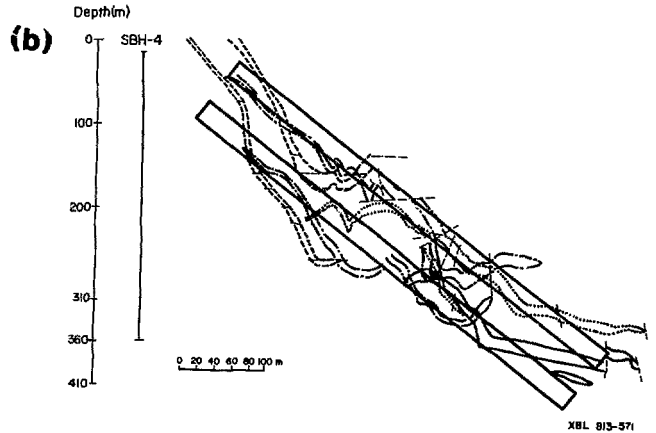

Fig. 6(b). Idealized geometry (bold line) of the superposed vertical sections -- double rectangles.

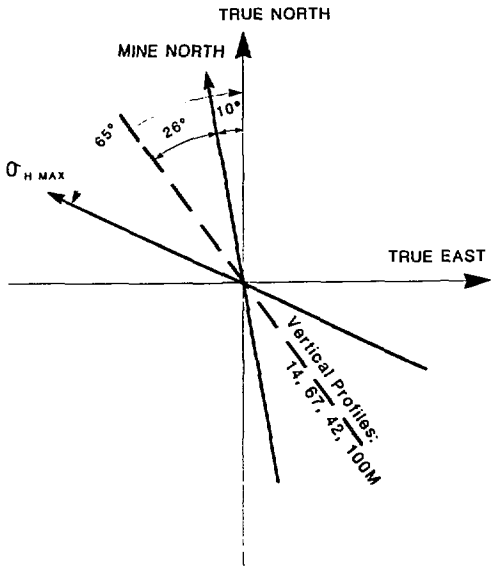

XBL 816-3232

Fig. 7. Orientations of maximum horizontal stress (as determined by hydraulic fracturing) and vertical profiles.

Applying regression analysis on the hydraulic fracturing experimental data (Doe et al., 1981), the distributions of maximum horizontal stress, $\sigma_{H_{max}}$, and minimum horizontal stress, $\sigma_{H_{min}}$ are found to be:

$$\sigma_{H_{max}} = 10^6 \, (10.03724 + 0.038801 \, z) \quad \text{(Pa)} \ ,$$

and

$$\sigma_{H_{min}} = 10^6 \, (1.69304 + 0.029868 \, z) \quad \text{(Pa)} \ ,$$

$$0 \leq z \leq 400 \text{ m} \ . \qquad (7)^*$$

The validity of the foregoing expressions is limited to the depth range of 0 to 400 m over which in situ stress was measured. Beyond the depth of 400 m, the relationship between the average horizontal stress and the vertical stress is assumed to lie within the global lower and upper bounds given by Hoek and Brown (1978). This relationship is depicted in Fig. 8.

For the depth range over which they were measured, the relationship between the stresses is given by:

$$K = \frac{\text{average horizontal stress}}{\text{vertical stress}} = \begin{cases} 264/z + 1.39 & 0 \leq z \leq 400 \text{ m} \\ 573/z + 0.61 & z \geq 400 \text{ m} \ . \end{cases} \qquad (8)$$

In the analyses of the horizontal sections, the maximum and minimum horizontal stresses at the 176 m and 360 m levels were calculated using Eq. (7). These secondary principal stresses in the horizontal plane were assumed to represent initial principal stresses that existed prior to any mining activity. Since the reference axes for the calculations coincided with the

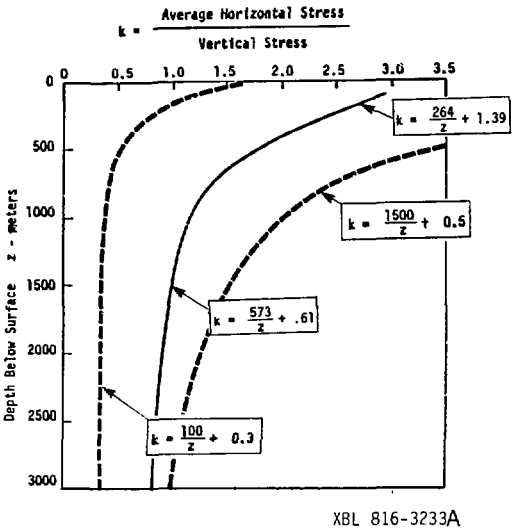

XBL 816-3233A

Fig. 8. Curves showing ratio between average horizontal stress to vertical stress as a function of depth. Dashed curves are bounding values according to Hoek and Brown (1978); solid curve represents values adopted for present work.

north and east orientations of the mine coordinate system, the principal stress components had to be resolved in relation to these reference axes. The resolved components of stress are shown in Figs. 9, 10, and 11; boundary conditions are also included. (Note that Figs. 9, 10, and 11 correspond to the discretizations in Figs. 14, 16(a), and 16(b), respectively.)

In the analyses of the vertical profiles, the horizontal stress components were found by rotating the principal stress components given by Eqs. (6) - (8) to the plane of the model. Boundary and loading conditions are shown in Figs. 12 and 13. (Conditions in Figs. 12 and 13 correspond to discretizations in Figs. 18(a) and 18(b), respectively.)

2.2.3 Material Properties

In the analyses, the rock was assumed to be an isotropic, linear elastic continuum with the following material properties:

Young's modulus, $E = 51.3$ GPa

Poisson's ratio, $\nu = 0.23$

Rock density, $\rho = 2622$ kg/m^3.

These properties are for intact core specimens of Stripa granite, as given by Pratt et al. (1977) for E and ν, and Swan (1978) for ρ.

For a 2-D isotropic, linear elastic medium the calculated stress concentration factor due to openings is, of course, independent of the elastic properties (Savin, 1961). In a 3-D solid the stress concentration factor will depend on Poisson's ratio (Sadowsky and Sternberg, 1949).

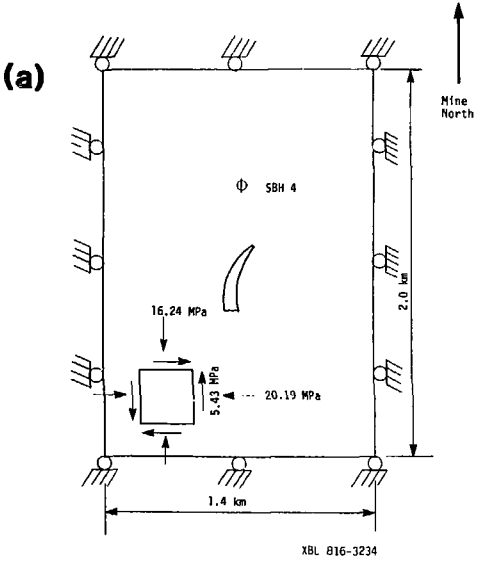

Fig. 9(a). Boundary and loading conditions of the 360 m level horizontal section -direct application of in-situ stresses.

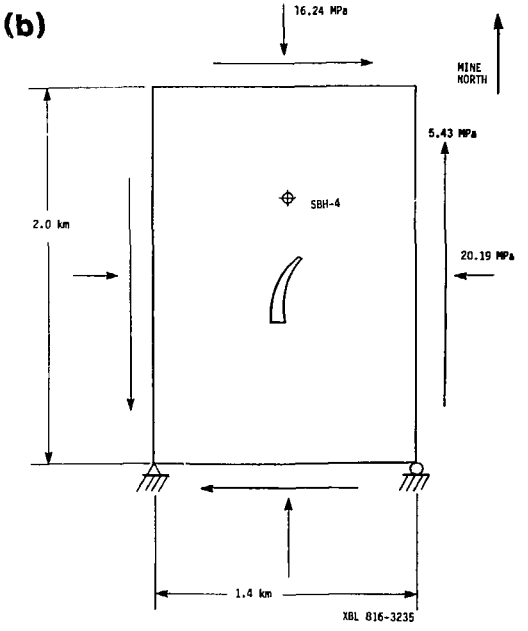

Fig. 9(b). Boundary and loading conditions of the 360 m level horizontal section - application of boundary forces.

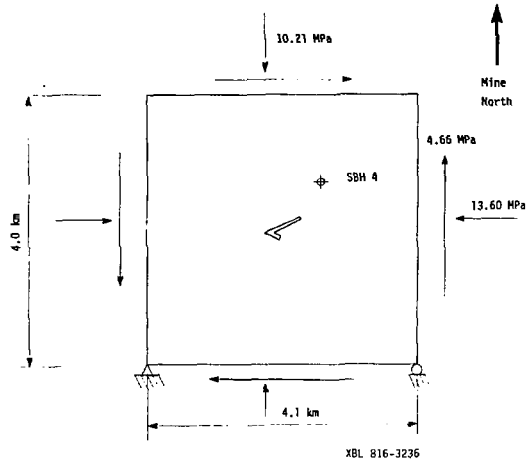

Fig. 10. Loading and boundary conditions of the 176 m level horizontal section.

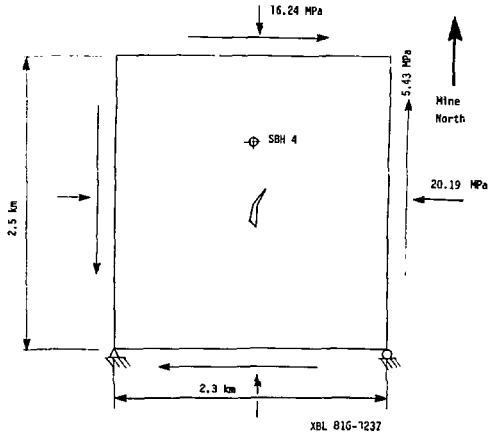

Fig. 11. Loading and boundary conditions of the 360 m level horizontal section.

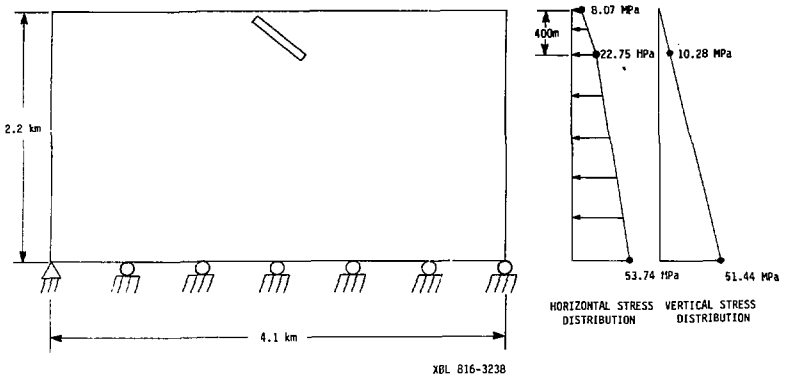

Fig. 12. Boundary and loading conditions of the vertical section with single rectangular opening.

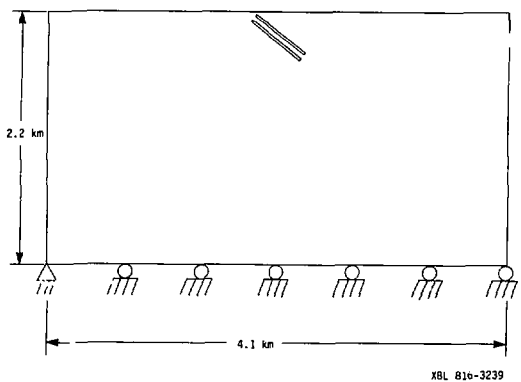

Fig. 13. Boundary conditions of the vertical section with double rectangular openings. Loading conditions are identical to those in Fig. 12.

3.0 RESULTS AND DISCUSSION

In this section, results are presented and discussed for (i) a test case with a relatively coarse 2-D mesh using two different methods for a consistency check of the computational techniques and (ii) four cases involving two horizontal and two vertical sections using finer 2-D meshes to simulate the field situation at Stripa.

3.1 Comparison of Two Loading Conditions

Sensitivity of stress distribution to changes in the two loading conditions--direct application of in situ stresses and the application of boundary forces, as discussed in Section 2.1--was investigated first. For this purpose, a configuration corresponding to the horizontal section at the 360 m level was employed.

The spatial discretization, comprising 308 nodes and 208 linear isoparametric quadrilateral elements, is displayed in Fig. 14. The two loading cases are show in Fig. 9. Stress distributions resulting from the loading conditions are shown in Fig. 15, from which one may conclude that they are almost identical.

Similar results, not shown in this report, were observed in stress distributions from the two loading cases in one of the vertical sections. On the basis of the evidence shown in Fig. 15, it may be inferred that consistent stress distributions can be calculated with either of the loading conditions tested, as expected from theory.

Since it is more expedient with available computer programs to employ the boundary loading technique, this approach was adopted in the actual stress analyses.

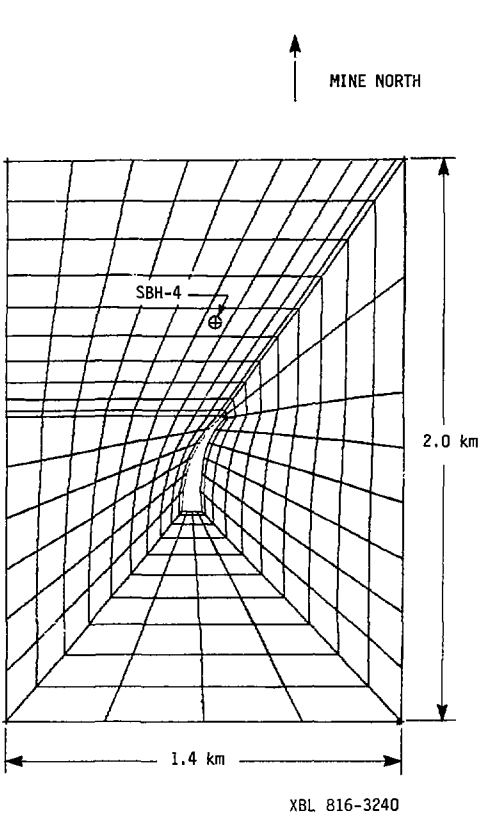

Fig. 14. Finite element mesh, 360 m level horizontal section.

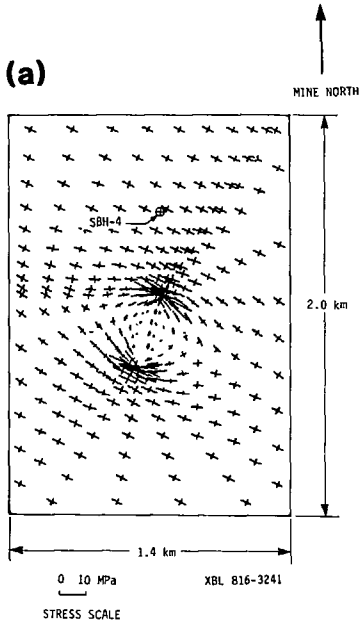

Fig. 15(a). Calculated principal stress distribution in the 360 m level horizontal section due to direct application of initial stresses.

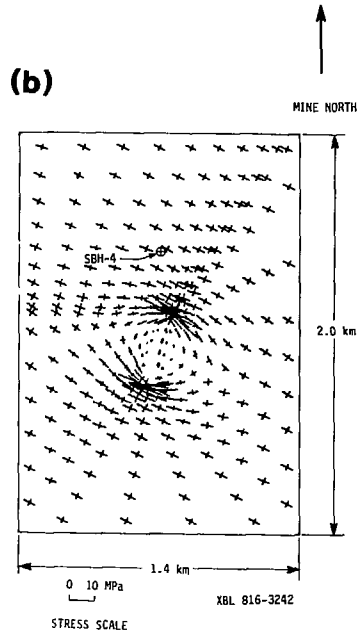

Fig. 15(b). Calculated principal stress distribution in the 360 m level horizontal section due to application of boundary forces.

3.2 Horizontal Sections

Discretizations of the horizontal sections at the 176 m and 360 m levels are displayed in Fig. 16; the internal openings represent excavated ore bodies. Details of discretizations are given in Table 1. Boundary and loading conditions are given in Figs. 10 and 11.

Calculated redistributed stress patterns at the 176 m and 360 m levels are shown in Fig. 17. A comparison between the initial stress with the redistributed stresses indicates that significant redistribution is confined to areas close to the openings. (In both 17(a) and 17(b), cross-like points far from the openings represent the magnitudes and orientations of the initial stresses.)

The calculation of stress concentration factors in terms of normal stress components at the location of SBH-4 is shown in Table 2. The results, which are very similar for the two sections, indicate that the presence of the mine openings has altered the in situ stress by 15% or less.

3.3 Vertical Sections

The finite element meshes of the vertical sections, where the mine openings were approximated by a single rectangle and by two rectangles, are displayed in Fig. 18. Details of discretization are given in Table 1. Boundary and loading conditions are shown in Figs. 12 and 13.

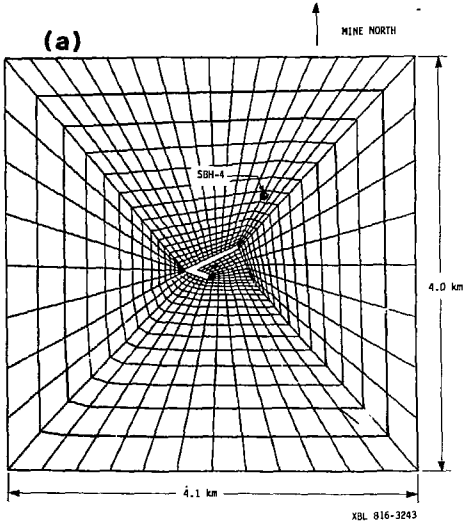

Fig. 16(a). Finite element mesh for the 176 m horizontal section.

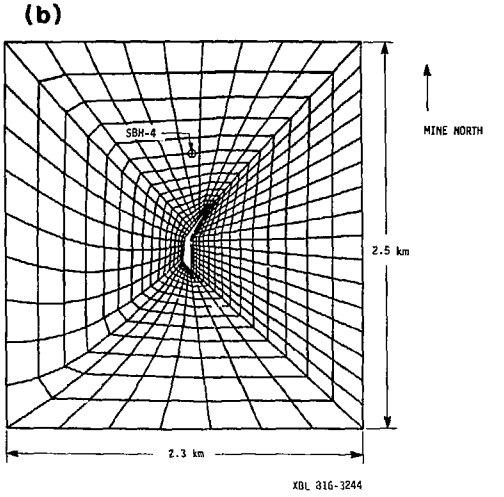

Fig. 16(b). Finite element mesh for the 360 m horizontal section.

Table 1. Discretization details.

Section	No. of Nodes	No. of Elements	Illustration
176 m H	768	724	Fig. 16 (a)
360 m H	656	615	Fig. 16 (b)
Single rectangle V	661	600	Fig. 18 (a)
Double rectangle V	806	723	Fig. 18 (b)

Note: H -- Horizontal
V -- Vertical

Table 2. Normal stresses and stress concentration factors at SBH-4, horizontal sections.

Level	σ_y (MPa)	σ_y^R (MPa)	SCF = $\frac{\sigma_y^R}{\sigma_y}$	σ_x(MPa)	σ_x^R (MPa)	SCF = $\frac{\sigma_x^R}{\sigma_x}$
176 m	13.60	15.10	1.11	10.21	8.72	0.85
360 m	20.29	21.94	1.09	16.22	14.51	0.89

Note: In labeling the stress components, positive y-axis corresponds to the mine-east direction and positive x-axis corresponds to the mine-north direction.

σ_x, σ_y are normal stresses deduced from hydrofracture measurements (Doe et al., 1981).

Superscript R refers to redistributed stresses.

SCF = stress concentration factor.

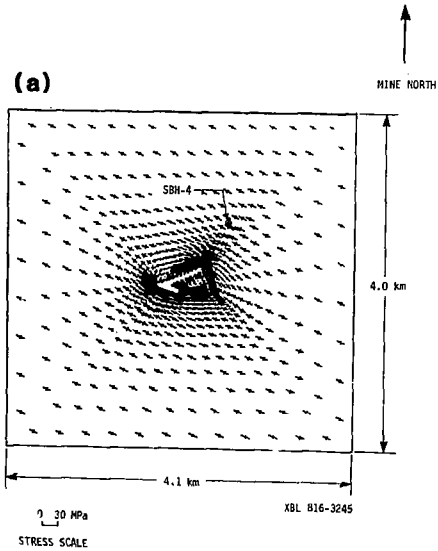

Fig. 17(a). Principal stress distribution in the 176 m level horizontal section.

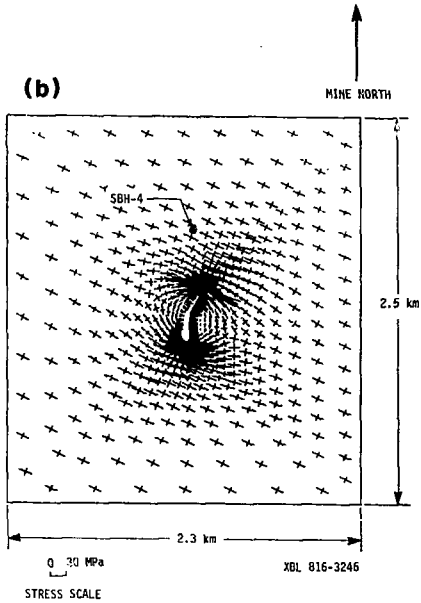

Fig. 17(b). Principal stress distribution in the 360 m level horizontal section.

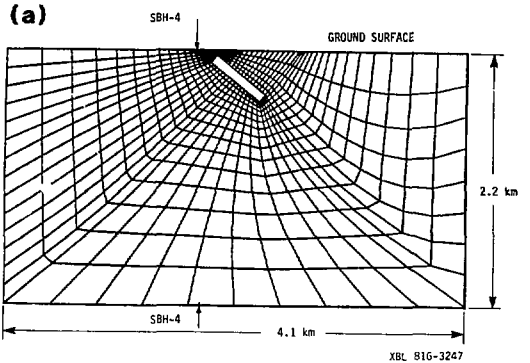

Fig. 18(a). Finite element mesh for the vertical section with single rectangular opening.

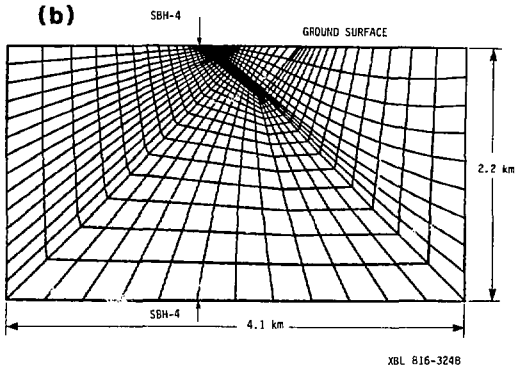

Fig. 18(b). Finite element mesh for the vertical section with double rectangular opening. Rock elements are put back between the openings.

Patterns of calculated redistributed stress are displayed in Fig. 19. Significant stress changes occurred from the ground surface down to about 200 m. Furthermore, the patterns of redistributed stresses outside the openings are practically independent of the number of rectangular openings.

From an inspection of plots of stress concentration factor (SCF) vs. depth given in Fig. 20, one can infer that at depths greater than 200 m the alteration of initial stresses is no more than 25%. At less than 200 m it is apparent that SCF increases fairly rapidly as the depth becomes shallower. This is discussed in the next section.

In the numerical models the reasonable assumption was made that the pre-mining principal stresses were vertical and horizontal. A comparison of the overcoring measuremnt with the calculated redistributed stresses was made (Fig. 21) to study whether the inclined angles of the overcoring principal stresses are consistent with this modeling assumption. Unfortunately, the scatter of the overcoring measurements obscures the answer to this question.

3.4 Discussion

The basic objective of the analyses was to estimate the effects of mining upon the redistribution of in situ stresses. The analyses were carried out via a series of two-dimensional approximations. Such approximations are quite conservative (in that they yield the upper bounds of changes in initial stress) because in two-dimensional projection the excavated areas appear to be closer to the SBH-4 hole than they are in reality (see Figs. 1 and 2). This is particularly true for the vertical sections.

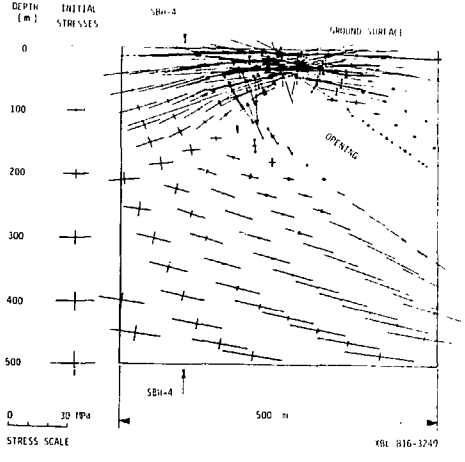

Fig. 19(a). Principal stress distribution in the vertical section with one rectangular opening. Depth and magnitude of initial stresses are shown on left. Arrows denote tension.

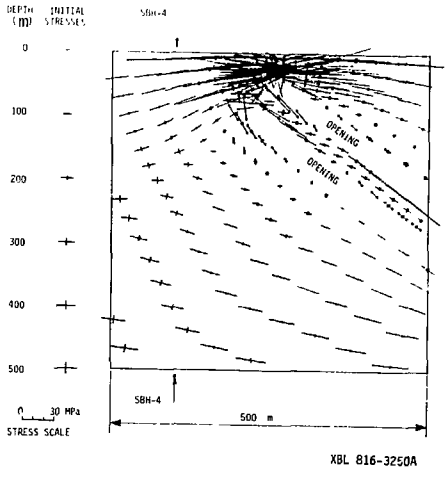

Fig. 19(b). Principal stress distribution in the vertical section with double rectangular openings. Depth and magnitude of initial stresses are shown on left. Arrows denote tension.

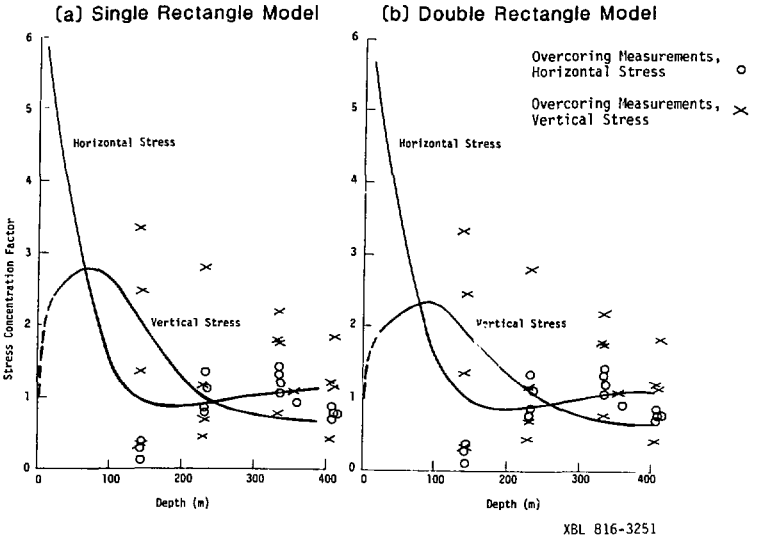

Fig. 20. Plots of stress concentration factors (calculated redistributed stress/initial stress) for horizontal and vertical stress components on the vertical plane at the SBH-4 hole vs. depth from ground surface. For comparison, the measured stresses from overcoring have been divided by the assumed pre-mining in situ stresses.

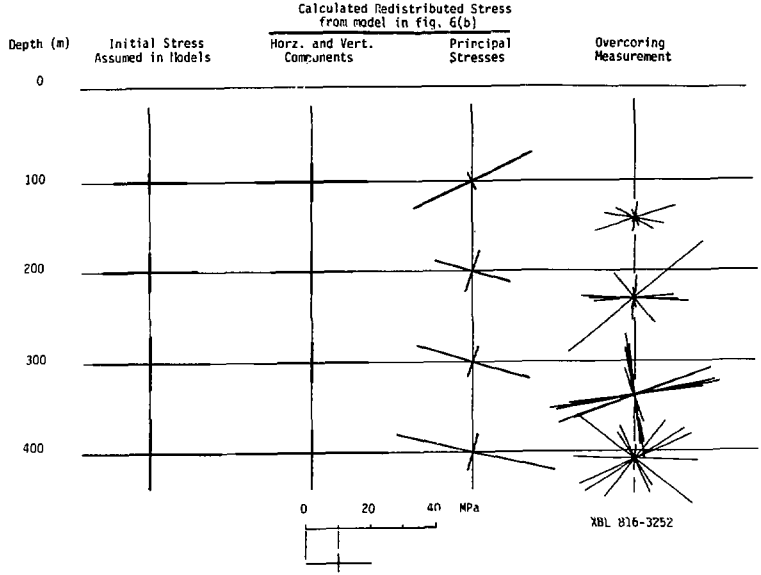

Fig. 21. Comparison of initial stress, calculated redistributed stress, and overcoring data.

The closest actual approach of the mining excavation to the SBH-4 borehole is about 350 m, at a depth of about 360 m; it is about 700 m from it at the surface. In the vertical models, the excavation is about 100 m from SBH-4 at a depth of 100 m. It is therefore not surprising that the calculated redistributed stresses for the vertical sections are much higher than the measured stresses close to the surface.

The calculation of in situ stress from field experiments, by either the overcoring or the hydraulic fracturing method, is always based on simplifying assumptions about the rock mass -- that it is, for example, homogeneous, intact, isotropic, and linear elastic. Such assumptions are usually not satisfied by field conditions. Results obtained from these tests are therefore always associated with errors due to field uncertainties. It is also possible that the in situ stress actually varies rapidly from point to point. The large scatter of the measurements (Fig. 21) provides some indication of the magnitude of these uncertainties. The measurement errors are likely to be largest near to the surface where, due to lower in situ stresses, more open fractures are likely.

These near-surface measurement errors and uncertainties in the vertical cases make it difficult to judge whether the large stress concentration factors at shallow depths really represent the in situ condition. These results, however, are of little concern because the underground experimental areas, the main region of interest, is below 300 m.

Results from the analyses of the horizontal sections indicate that the maximum change in the in situ stress is about 15%; in the vertical sections at depths greater than 200 m, it is about 25%. These changes are

relatively small compared with the uncertainties in the measured stress. Likewise, the calculated changes in stress orientation for the horizontal sections and for the vertical sections below a depth of 200 m are comparable with the scatter of the overcoring measurements.

4.0 CONCLUSIONS

On the basis of the present study, the following conclusions may be drawn: (i) At depths between 200 m and 400 m, encompassing the underground test horizon, the mining-induced stress concentrations are relatively insignificant when the uncertainties in the in situ stress measurements are considered; (ii) differences between orientations of principal stresses from finite element modeling using vertical sections and those from overcoring measurements are comparable with the variations among different overcoring measurements at approximately the same depth; (iii) further elaboration of the numerical modeling of far-field stress appears unwarranted; and (iv) for the purpose of near-field in situ stress calculations, the vertical stress due to overburden weight, along with horizontal stresses measured by hydrofracturing at SBH-4, can be taken as the inital, pre-mining far-field stress.

ACKNOWLEDGMENTS

The authors gratefully acknowledge the following individuals: P.A. Witherspoon for encouragement; N.G.W. Cook for general guidance in rock mechanics; S. Flexser, P. Nelson, R. Rachiele, and W. Thur for helping to assemble maps and profiles; D.E. Wedge for assistance in computer plotting and computation of coordinate transformation for stress tensors; M. Kubacki and W. Wong for preparing some of the illustrations; and P. MacLean and D. Watkins for reviewing the draft. Special mention should be made of T. Doe for providing the results of in situ stress measurements. The authors, however, assume sole responsibility for the calculations reported.

This work was supported by the Assistant Secretary for Nuclear Energy, Office of Waste Isolation of the U. S. Department of Energy under contract DE-AC03-76SF00098. Funding for this project is administered by the Office of Nuclear Waste Isolation at Battelle Memorial Institute.

REFERENCES

Chan, T., 1979. Thermal and Stress Analyses for a High-Level Radioactive Waste Vault in Crystalline Rock. Technical record TR-69, Storage and Disposal Branch, Whiteshell Nuclear Research Establishment, Atomic Energy of Canada Limited, Pinawa, Manitoba, Canada.

Chan, T. and N.G.W. Cook, 1979. Calculated Thermally Induced Displacements and Stresses for Heater Experiments at Stripa, Lawrence Berkeley Laboratory report LBL-7061, SAC-22, Berkeley, California.

Chan, T., M. Hood, and M. Board, 1980. "Rock Properties and Their Effect on Thermally-Induced Displacements and Stresss," presented at the Am. Soc. Mech. Eng. 1980 Energy Technology Conference and Exhibition, New Orleans, Louisiana, February 3-7, 1980. Lawrence Berkeley Laboratory report LBL-20517, Berkeley, California.

Chan, T., N. Littlestone, and O. Wan, 1980. "Thermomechanical Modeling and Data Analysis for Heating Experiments at Stripa, Sweden." In The State of the Art in Rock Mechanics, Proc. 21st U. S. Symp. on Rock Mechanics, Rolla, Missouri, May 28-30, 1980, Ed. D. A. Summers, pp. 16-25.

Doe, T.W., K. Ingevald, L. Strindell, and B. Hamison, 1981. "Hydraulic Fracturing and Overcoring Measurements in a Deep Hole at the Stripa Test Mine, Sweden," to be presented at U.S. 22nd Rock Mechanics Symposium, MIT, Cambridge, Massachusetts.

Hoek, E., and E.T. Brown, 1978. "Trends in Relationships Between Measured In-Situ Stress and Depth." International Journal of Rock Mechanics and Mining Sciences, Vol. 15, No. 4, pp. 211-216.

Olkiewicz, A., J.E. Gale, R. Thorpe, and B. Paulsson, 1979. Geology and Fracture System at Stripa. Lawrence Berkeley Laboratory report LBL-8907, SAC-21, Berkeley, California.

Pratt, H., T.A. Schruaf, and L. Bills, 1977. Summary Report - Thermal and Mechanical Properties of Granite - Stripa, Sweden. Report No. TR 77-92, Terra Tek, Inc., Salt Lake City, Utah.

Sadowsky, M.A., and E. Sternberg, 1949. "Stress Concentration Around a Triaxial Ellipsoidal Cavity." Journal of Applied Mechanics, Vol. 16, pp. 149-159.

Savin, G.N., 1961. Stress Concentration Around Holes, Pergamon Press, New York.

Swan, G., 1978. The Mechanical Properties of Stripa Granite, Lawrence Berkeley Laboratory report LBL-7074, SAC-03, Berkeley, California.

Witherspoon, P.A., N.G.W. Cook, and J E. Gale, 1981. "Geological Storage of Radioactive Waste: Field Studies in Sweden." Science, Vol. 211, pp. 894-900.

Zienkiewicz, O.C., 1977. The Finite Element Method, 3rd edition, London: McGraw-Hill.

APPENDIX: CONTOUR PLOTS OF STRESS CONCENTRATION FACTORS

This appendix consists of a set of contour plots of the stress concentration factors, defined as the ratio of the horizontal (or vertical) component of calculated redistributed stress in the presence of the mine openings(s) to the corresponding component of assumed pre-mining stress. All four finite element models reported in the main text are illustrated.

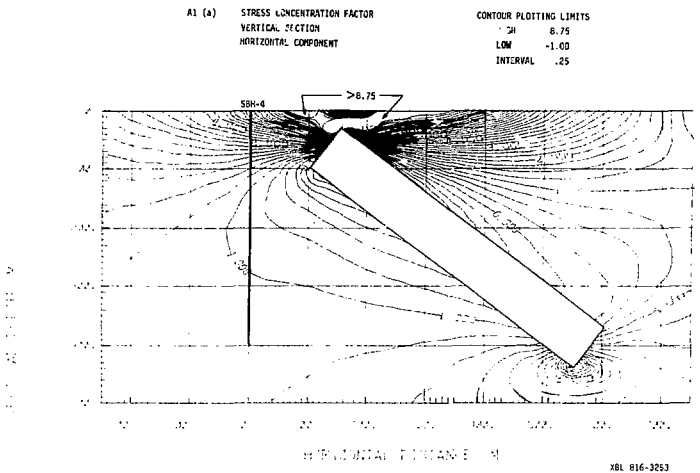

Fig. A1(a). Stress concentration factor contours, vertical section, one rectangular opening-horizontal stress component.

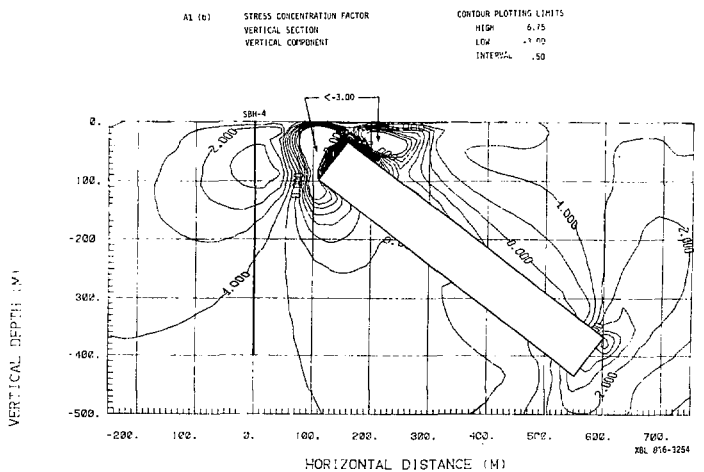

Fig. A1(b). Stress concentration factor contours, vertical section, one rectangular opening-vertical stress component.

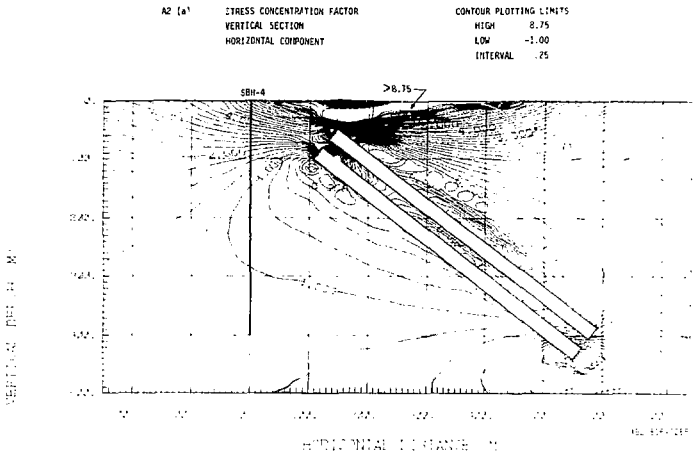

Fig. A2(a). Stress concentration factor contours, vertical section, two rectangular openings - horizontal stress component.

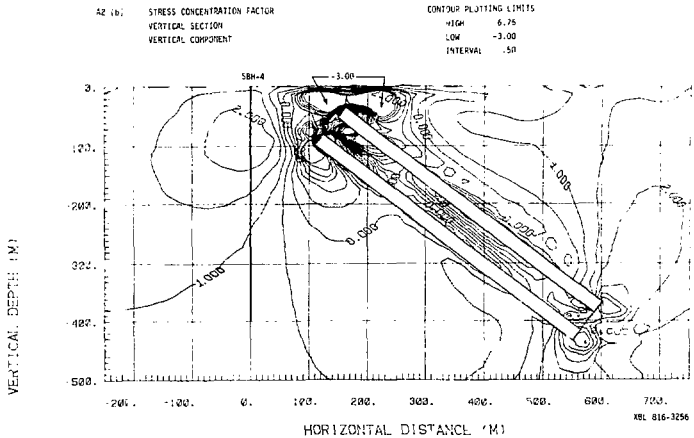

Fig. A2(b). Stress concentration factor contours, vertical section, two rectangular openings - vertical stress component.

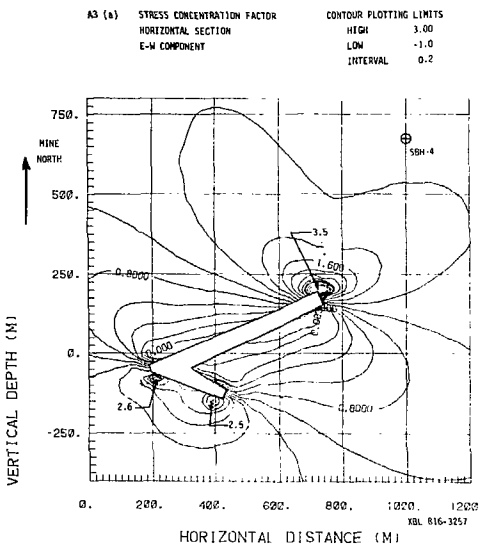

Fig. A3(a). Stress concentration factor contours, horizontal section 176 m level - E-W stress component.

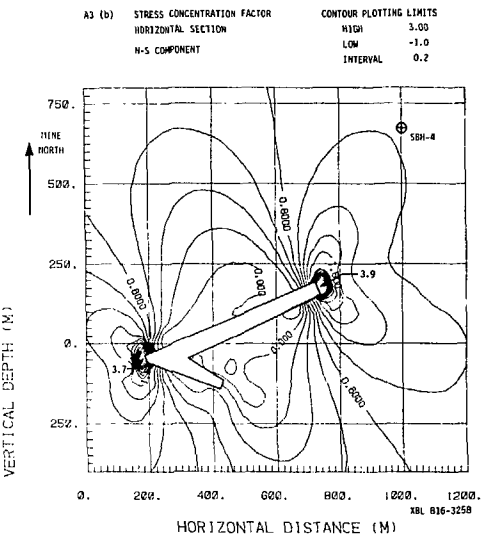

Fig. A3(b). Stress concentration factor contours, horizontal section 176 m level - N-S stress component.

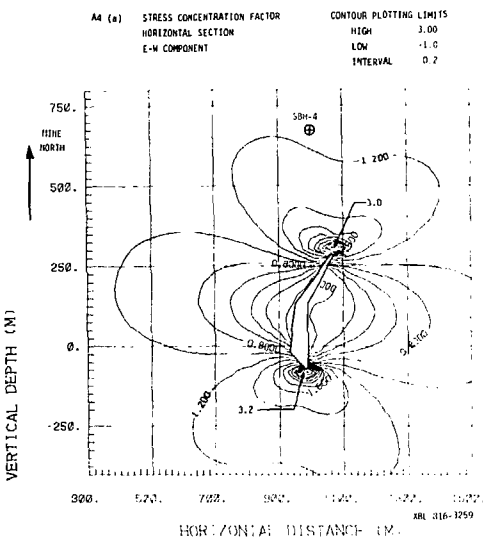

Fig. A4(b). Stress concentration factor contours, horizontal section, 340 m level - N-S stress component.

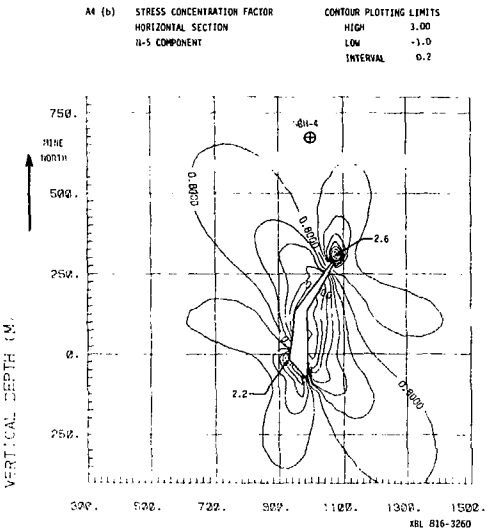

Fig. A4(a). Stress concentration factor contours, horizontal section, 340 m level - E-W stress component.